Nanoparticles Infiltration into SOFC Cathode Backbones

Julian Dailly, Aude Delrue, Marie Ancelin, Mathieu Marrony

European Institute For Energy Research (EIFER), Karlsruhe 76131, Germany

Intermediate Temperature Solid Oxide Fuel Cells (IT-SOFCs) with yttrium stabilized zirconia electrolyte were fabricated by the impregnation of nanoparticle promoters into specific backbone cathodes: electronic conductor $La_{0.8}Sr_{0.2}MnO_3$, ionic conductor $Sm_{0.2}Ce_{0.8}O_{2-\delta}$ and mixed ionic and electronic conductor $Nd_{1.95}NiO_{4+\delta}$. The electrochemical performances of the symmetrical half-cells and single cells were improved using impregnated cathodes. The electrochemical measurements showed that a MIEC backbone is more efficient than a pure electronic or a pure ionic one. The highest area specific resistance was given by $La_{0.8}Sr_{0.2}MnO_3$-impregnated samples (ASR_{elec} = 1.15 $\Omega.cm^2$) at 700°C. At the same temperature, the lowest resistance was measured on a $Pr_2NiO_{4+\delta}$ impregnated into an $Nd_{1.95}NiO_{4+\delta}$ backbone (ASR_{elec} = 0.26 $\Omega.cm^2$). Complete single IT-SOFCs with and without infiltrated air electrodes have been then manufactured and the infiltration improved clearly the efficiency of the cell, more than 6% in the temperature range 650-750°C without specific optimization.

Introduction

The electrochemical energy resulting from the combination of hydrogen and oxygen to produce water could be converted into electrical energy and heat through fuel cells. This reaction takes place in a wide range of temperature (80 to 1000°C). The high efficiency comes from the Solid Oxide Fuel Cell operating at between 800 and 1000°C. Its main benefit is its ability to produce at the same time electricity and heat. Because of the high degradation rate of materials at high temperature (chemical reactivity, bad mechanical strength, expensive interconnector materials…), it has been necessary to soften the operating condition to increase the tolerance of materials: the main idea is to decrease the operating temperature to 700°C or lower. Unfortunately, the kinetics being thermally activated performances decreases drastically with temperature. The air side is the most critical point because of a huge increase of the cathode over potential while decreasing the temperature. It is crucial to find new materials or new electrode design to limit the polarisation resistance of the air electrode.

The infiltration of nanoparticles into a specific backbone could theoretically improve the electrochemical performance of the air electrode, and thus of the cell (1-2). This method consists of the elaboration of a precursor's solution which is then impregnated into the porosity of an electrode. Basically, nano-sized electrocatalysts are introduced into a porous structure. The microstructure could be optimized through this method that would increase the length of triple-phase boundary (TPB) between the electrolyte,

electrode, and gas phase (3-4). This process allows advantages, such as increase the specific area, improve the electrochemical process and reduce thermal mismatches due to different thermal expansion coefficients (TEC) (5). Impregnation was proven to be a useful technique to optimize the electrode structure (6). By infiltrating a second phase material into a backbone support, the Nano-scale particles of the second phase material could be yielded after sintering (7).

Among cathode compounds for IT-SOFCs, $La_{0.8}Sr_{0.2}MnO_3$ perovskite (LSM) is a classical electronic conductor (8), widely used for SOFCs. Chemically stable at high temperature (800°C), this material exhibits a very low ionic conductivity and high activation energy for oxygen dissociation, and is considered as a pure electronic conductor. LSM as a cathode has thus limited applications for IT-SOFC (9-10). For the configuration LSM/YSZ/LSM, the literature shows an ASR_{elec} of 7.82 $\Omega.cm^2$ at 700°C (6).

The nickelate materials are good mixed ionic and electronic conductors (MIEC). For instance, $Nd_{1.95}NiO_{4+\delta}$ (NdN) (1) is stable and does not significantly react with the YSZ electrolyte (11). Also, power densities above 500 $mW.cm^{-2}$ have been reported by Lalanne, et al at 700°C and 0.7 V with $Nd_{1.95}NiO_{4+\delta}$ cathode on YSZ electrolyte (12). Few people have work on the impregnation of nickelates into porous backbones (13-14-15), even if those materials seems to have particularly advantageous properties like a good electronic conductivity (σ=100 $S.cm^{-1}$) or a high diffusion coefficient of oxygen 5.10^{-8} $cm^2.s^{-1}$ at 700°C in case of NdN. For $Nd_2NiO_{4+\delta}$/YDC/8YSZ/YDC/$Nd_2NiO_{4+\delta}$ configuration the literature shows ASR_{pol} = 0.5 $\Omega.cm^2$ at 700 °C (16). The praseodymium nickelate oxide $Pr_2NiO_{4+\delta}$ is another material of the Ruddlesden-Popper family with the K_2NiF_4-type structure. This rare-earth nickelate appears as a promising compound cathode with a large oxygen diffusivity values and a large amount of interstitial oxygen, reflected by the δ value ($\delta \sim 0.22$ at room temperature) (17-18).

Other materials, $Sm_{0.5}Sr_{0.5}CoO_{3-\delta}$ (SSC) exhibits better electronic conductivity than the nickelates, thus potentially improving the electrochemical properties of these cathodes (19). SSC compound is an excellent cathode for low temperatures, with a high surface oxygen exchange rate and bulk oxygen ion diffusion coefficient and a good catalyst for oxygen reduction (20). Another composition $Sm_{0.2}Ce_{0.8}O_{2-\delta}$ (SDC) is an ionic conductor and has been already used as electrolyte in SOFCs technologies (21). Some people have already worked on SDC ion-impregnated, for example the performances of single cells with SDC infiltrated into LSM cathodes have been reported. Chen et al. have compared three LSM-based cathodes configurations, pure LSM, LSM/YSZ composite prepared by solid mixing and LSM/SDC prepared by ion-impregnation process, on YSZ-based half-cell. Whereas the LSM/YSZ composite-based cell appeared to be the most efficient at high temperature (800°C), better performance was achieved with the LSM/SDC cathode at lower operating temperatures (maximum power density 0.4 $W.cm^{-2}$ at 600°C) (22). A maximum power density of 0.5 $W.cm^{-2}$ at 600°C was reported by Tian and al. with a cell based on SDC electrolyte with SDC nanoparticles impregnated in both Ni/SDC and LSM electrodes (23).

Ceria and doped-ceria are materials known for their good oxidation catalytic properties and high ionic conductivity (24). The investigations indicate that the impregnation of nano-sized ceria-based ionic conducting materials accelerates the oxygen

dissociation and the diffusion processes. The enhancement in O_2 reduction kinetics is related to the high electro-catalytic effect and the high surface areas of the impregnated phase, as well as the enhancement of the triple phase boundaries for the O_2 reduction (25). Indeed, if the impregnated particles get connected, they will form a continuous way for oxygen ion conduction, at the final, TPB is extended from the cathode / electrolyte interface to the bulk of the cathode. Among the ceria-based ionic conducting materials, Samarium doped Ceria was found to exhibit the highest oxygen-ion conductivity at certain fixed doping levels (26).

Our strategy consisted in the impregnation of such Nano-sized efficient promoters into specific porous backbones. The goal of this study is to show the efficiency of the impregnation process in order to decrease ASR_{pol}, using a reference material like LSM and more innovative compounds like mixed ionic and electronic conductors. Three different backbone materials were coated onto Yttria-stabilized zirconia pellets: $La_{0.8}Sr_{0.2}MnO_3$ (LSM) as pure electronic conductor, $Sm_{0.2}Ce_{0.8}O_{2-\delta}$ (SDC) as pure ionic conductor and $Nd_{1.95}NiO_{4+\delta}$ (NdN) as mixed ionic and electronic conductor (MIEC). The electrochemical activities of several compositions were then studied as promoter infiltrated inside the backbones: $Sm_{0.5}Sr_{0.5}CoO_{3-\delta}$ (SSC), $Sm_{0.2}Ce_{0.8}O_{2-\delta}$ (SDC), CeO_2, $Nd_{1.95}NiO_{4+\delta}$ (NdN), $Pr_{1.97}NiO_{4+\delta}$ (PrN), and $La_{0.8}Sr_{0.2}MnO_3$ (LSM).

Experimental

Symmetrical Half-cells

TABLE I. Sintering cycles used for the different backbones.

Backbone	Sintering cycle	Symmetrical half-cell
$Nd_{1.95}NiO_{4+\delta}$	1150°C / 1h	
$La_{0.8}Sr_{0.2}MnO_3$	1100°C / 1h	
$Sm_{0.2}Ce_{0.8}O_{2-\delta}$	900°C / 1h	
$Nd_{1.95}NiO_{4+\delta}$	1150°C / 1h	

The symmetrical pellets were prepared using YSZ commercial powder (TOSOH) by uniaxial pressing (40 MPa) and sintered for 10 hours at 1450°C under air. The sintered pellets had a diameter of 14.5mm (surface area of 1.76cm²) and a density above 95%. Backbone cathodes were prepared by screen-printing on both sides of YSZ pellets $Nd_{1.95}NiO_4$ (NdN) (Marion Technologies), $La_{0.8}Sr_{0.2}MnO_3$ (LSM) (Marion Technologies) or $Sm_{0.2}Ce_{0.8}O_{2-\delta}$ (SDC) (Sigma Aldrich) materials. The screen-printing inks were prepared using 50%wt of ceramic powder and 50%wt of an organic vehicle (6wt% ethylcellulose in Terpineol). The sintering of the backbone is performed at high

temperature, which ensures a good bonding between the backbone and the electrolyte, a good connection between the particles for the effective conduction of electrons and/or oxygen ions, and the structural stability of the cathode. The NDN backbone used to manufacture the complete cells were elaborated following the same screen-printing process on commercial SOFC half-cells (Ni-YSZ/YSZ; 60x60mm²). According to the backbone, different heat treatments were used as shown in Table I.

Promoter Solutions

Promoter solutions shown in figure 1 were made by mixing stoichiometric amounts of nitrate precursor solutions (see Table II). Ethanol was added to improve the wetting of the solutions.

Figure 1. Promoter's solution.

TABLE II. Composition of the different promoter solutions.

Promoter	Precursors
$Sm_{0.2}Ce_{0.8}O_{2-\delta}$	$Sm(NO_3)_3.6H_2O$; $Ce(NO_3)_3.6H_2O$ (Sigma-Aldrich)
$Sm_{0.5}Sr_{0.5}CoO_{3-\delta}$	$Sm(NO_3)_3.6H_2O$; $Sr(NO_3)_2$; $Co(NO_3)_2 \cdot 6H_2O$ (Sigma-Aldrich)
CeO_2	$Ce(NO_3)_3.6H_2O$ (Sigma-Aldrich)
$Nd_{1.95}NiO_{4+\delta}$	$Nd(NO_3)_3.6H_2O$ (Alfa Aesar) ; $Ni(NO_3)_2.6H_2O$ (Sigma-Aldrich)
$Pr_{1.97}NiO_{4+\delta}$	$Pr(NO3)_3.6H_2O$ (Alfa Aesar) ; $Ni(NO_3)_2.6H_2O$ (Sigma-Aldrich)
$La_{0.8}Sr_{0.2}MnO_3$	$La(NO_3)_3.6H_2O$ (Alfa Aesar) ; $Sr(NO_3)_2$; $Mn(NO_3)_2.4H_2O$ (Sigma-Aldrich)

Impregnation Process

The impregnation into the backbone NdN, LSM and SDC was done by capillary action under vacuum.

Two impregnation processes were used and compared:

- The first one named painting consisted to put few drops of the promoter solution on the backbone and then spread it on the surface with a paintbrush. The process is made on the two faces of the pellet, and then a vacuum step is performed to help the infiltration process. This, method has also been applied to infiltrate the promoter on the air electrode of the complete cells.

- The second method, namely vacuum-assisted method, consisted in firstly vacuuming the sample, and then to drop the promoter solution on the surface of the sample.

Both processes were followed by a drying step at 110°C for 10 min and a subsequent heat treatment at 500°C for 30 min was used to remove the nitrates between each impregnation cycle. The loading amount of the promoters can be increased by repeating the impregnation and the drying steps at 110°C and 500°C. Finally a generic heat treatment at 850°C for 1 hour has been used for all the promoters. For convenient reasons, the painting process has been applied to impregnate the complete fuel cells.

During the experiments on symmetrical half-cells, the amount of promoter loading was between 0wt% and 20wt%. The results are then given in percentage of impregnation which corresponds to the ratio of the promoter by mass relative to the mass of backbone. It should be noted that the mass of backbone is the same for each samples.

Characterizations

Symmetrical half-cells were tested in a dedicated furnace using a simple spring-assisted sample holder. The current collection was performed with gold meshes (area of 1.76cm²) on both sides of the symmetrical samples. All the measurements have been performed under non-humidified air. Electrochemical Impedance Spectroscopy measurements were obtained over the frequency range from 0.31 to 103 Hz using a Solartron FRA 1255 and the software ZPlot®.

Single cells were tested in a Fiaxell® Open Flange fuel cell test bench at 600 °C with non-humidified hydrogen as fuel and non-humidified compressed air as oxidant. The current collection was performed using gold wires connected to a gold mesh (ϕ37mm) at the air side and nickel wires connected to a nickel mesh (70x70mm²) at the fuel side. Electrochemical measurements (IV and IP curves) were carried out with the software CorrWare®. Electrochemical Impedance Spectroscopy measurements were obtained over the frequency range from 0.31 to 103 Hz using a Solartron FRA 1255 and the software ZPlot®. External morphologies of the cell were studied by electron microscopy in a field-emission scanning secondary electron microscope.
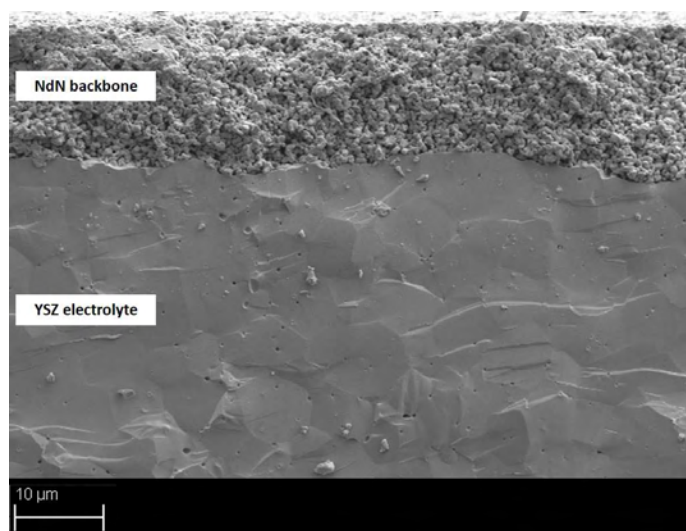
Results and Discussion

Figure 2. SEM observation of a symmetrical half-cell.

Figure 2 presents the global microstructure of a symmetrical half-cell composed of an YSZ electrolyte and a NdN backbone. The electrolyte is well densified whereas the backbone presents a homogeneous porosity required for an electrode, especially for the infiltration process. The thickness of the backbone is around 12 µm and the estimated porosity about 25%. The interface between cathode and electrolyte seems to be good: no delamination between both layers is observed and the electrode is well attached to the electrolyte pellet.

Electrochemical Measurements

Electrical resistance values of the electrode layer (ASR_{elec}) were deduced from typical Nyquist plots of the impedance data shown in the figure 3. The high-frequency intercept corresponds to the Ohmic resistance (ASR_{Ω}), whereas the low-frequency intercept is the total resistance of the half-cell (ASR_{tot}). Thus the polarization resistance (ASR_{pol}) of the electrodes is deduced from the two previously defined resistance by following the equation 1:

$$ASR_{pol} = ASR_{tot} - ASR_{\Omega} \qquad [1]$$

Then, the polarization resistance is composed of the contribution of both identical electrodes of the symmetrical half-cell samples. As both electrodes are identical, we can simply deduce that they have the same contribution so the contribution of one air electrode is calculated using the equation 2:
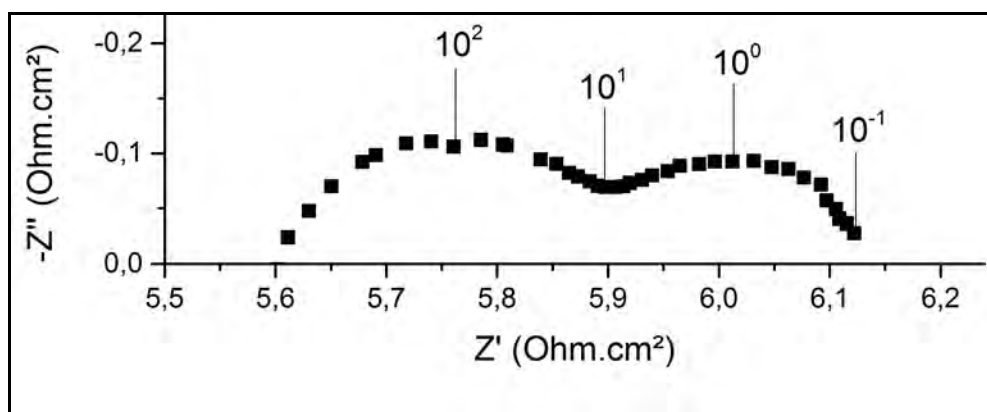
$$ASR_{elec} = \tfrac{1}{2} * ASR_{pol} \qquad [2]$$

Figure 3. Impedance diagram at 700°C of NdN backbone impregnated by PrN.

Comparison between the Two Processes of Impregnation

A comparison has been made between the two impregnation processes (the painting method and the vacuum-assisted impregnation method) to see which one leads to the most efficient performances: the polarization resistance of 2 NdN backbones impregnated with SSC and 2 NdN backbones impregnated with SDC with similar promotor loadings are displayed on the figure 4. For both compositions, the ASR_{elec} is around two times lower for the vacuum-assisted impregnation method than for the painting method (for

instance, ASR_{elec}=0.64 Ω.cm² and ASR_{elec}=1.38 Ω.cm² at 700°C for SSC samples, respectively), which indicates that the second process is not the most suitable for a good infiltration. It shows that the vacuum-step is required before the introduction of nanoparticles, most probably to facilitate the introduction of the promoter solution inside the porosity by capillarity. The classic vacuum-assisted impregnation process has thus been used to infiltrate all the symmetrical half-cells.
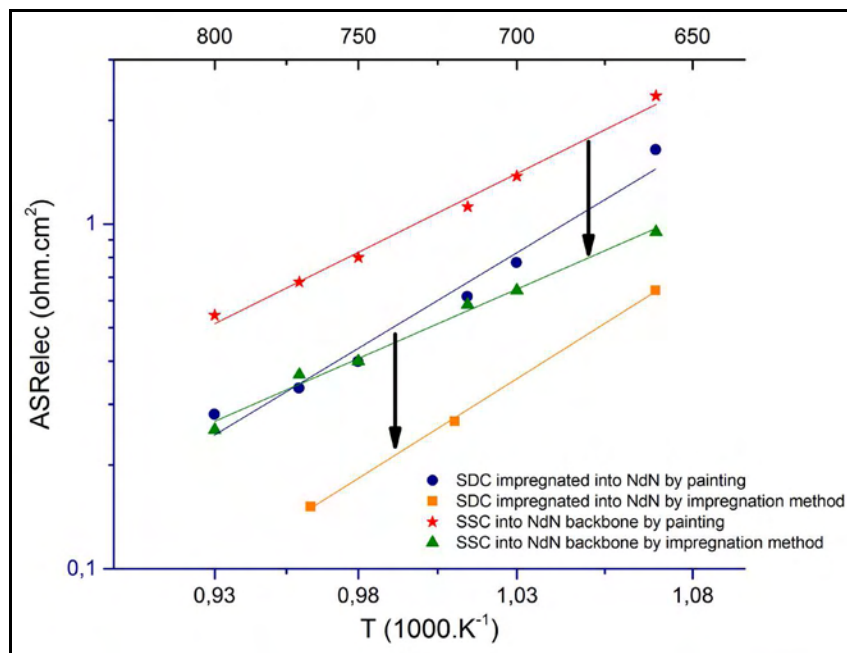

Figure 4. Evolution of the ASR_{elec} versus the two methods of impregnation.

NdN Backbone

NdN backbones have been impregnated with different promoters and various promoter loadings. Figure 5 represents the ASR_{elec} calculated as a function of the loading of promoter inside its backbone. It seems that a promoter loading around 10% is a good compromise for all configurations. 10% of promoter's loading has been used in the following results presented in this paper.

Except for the LSM-based samples, the ASR_{elec} has been drastically reduced (more than 70%) in comparison with the ASR_{elec} of the non-impregnated NdN backbone (black line on figure 5). The infiltration of a pure electronic conductor probably reduces the interface gas / ionic conductor which lower the electrochemical activity of the electrode layer.

A comparative study has been conducted between different promoter compositions into the same NdN backbone. Figure 6 presents the variation of ASR_{elec} of those combinations in a temperature range of 660 – 800°C. The highest ASR_{elec} (ASR_{elec}=2.63 Ω.cm² at 700°C) is reported for the reference sample which is a NdN backbone without promoter, and the LSM-impregnated sample which is closed to the reference. Except for the LSM, the impregnation decreases drastically the ASR_{elec} compared to the reference. Moreover, it should be noted that the impregnation of NdN promoter inside a NdN

backbone decreases the ASR_{elec} (ASR_{elec}=0.49 $\Omega.cm^2$), which clearly shows the high electrochemical advantage to Nano-structure the air electrode. Both observations validate the interest of using the impregnation process to reduce the polarization resistance of an electrode. For a temperature of 700 °C the lowest ASR_{elec} has been measured on the PrN-impregnated sample (ASR_{elec}=0.26 $\Omega.cm^2$).
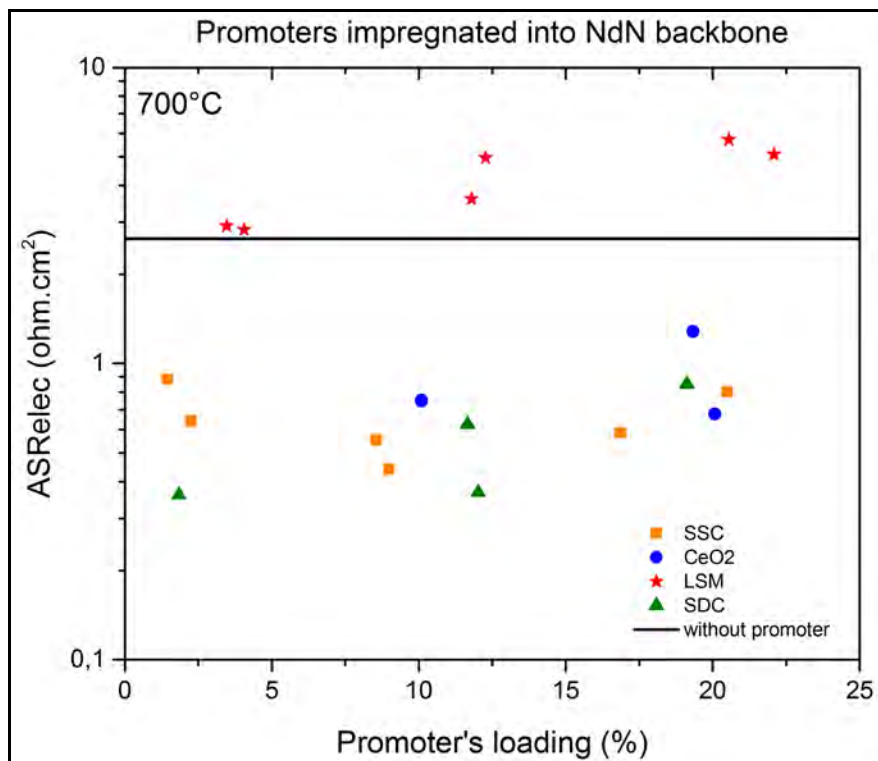

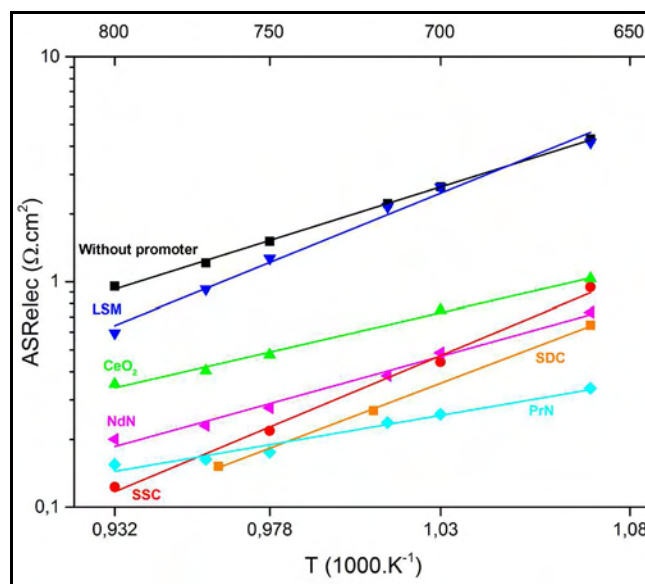Figure 5. Evolution of the ASR_{elec} at 700°C versus promoter's loading into NdN backbone.

Figure 6. Evolution of the ASR_{elec} versus temperature of different promoters into NdN backbone.

Figure 7 shows the microstructure of a symmetrical half-cells with a backbone impregnated with SDC promoter. We can observe the presence of nanometric SDC nodules in the porosity of the NdN backbone. According to EDX mapping (figure 8), it can be seen a homogeneous repartition of the promoter inside the electrode layer (Nd and Sm element from the backbone and the promoter, respectively).
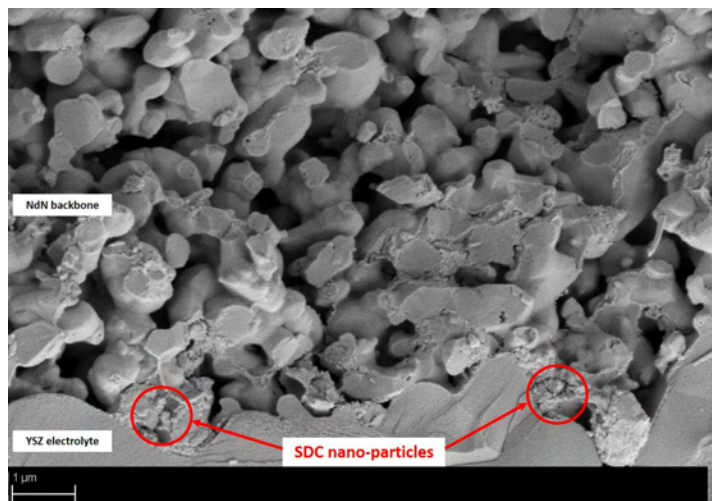

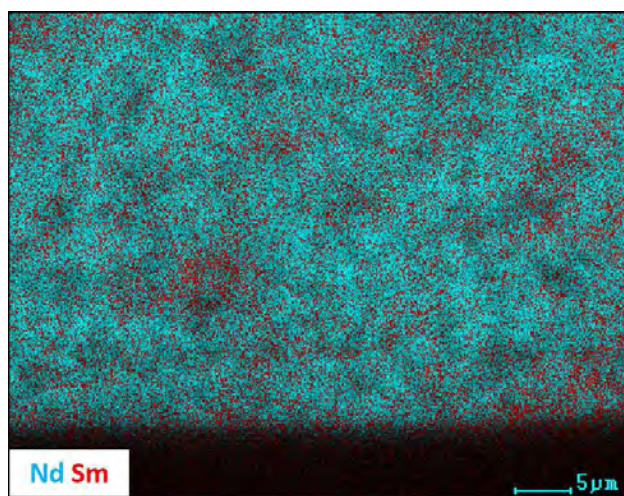Figure 7. SEM observation of SDC Nanoparticles into an NdN backbone.

Figure 8. EDX mapping (Nd and Sm element) of a NdN backbone impregnated with SDC promoter.

In order to study the influence of the nature of the backbone on the electrode properties, two other compositions LSM and SDC have been investigated as air electrode backbone.

LSM Backbone

Figure 9 presents the thermal variation of the ASR_{elec} for the LSM backbone symmetrical half-cells. One sample has been measure without promoters as reference, whereas the two other samples were impregnated with NdN and SDC promoters. As

already observed previously, the infiltrated samples have a lower ASR_{elec} than the reference without infiltration. At 700°C, electrode resistances ASR_{elec}=0.87 $\Omega.cm^2$ and ASR_{elec} of 3.19 $\Omega.cm^2$ have been measured on the SDC-impregnated and the NdN-impregnated LSM backbone, respectively. The values are higher than in the case of the MIEC backbone NdN (ASR_{elec} about 0.4 $\Omega.cm^2$ for both), showing that a MIEC backbone is more efficient than a pure electronic one. It can be deduced that the ionic conductivity of the backbone helps considerably the ionic conduction to the electrolyte layer, and thus improve the overall efficiency.
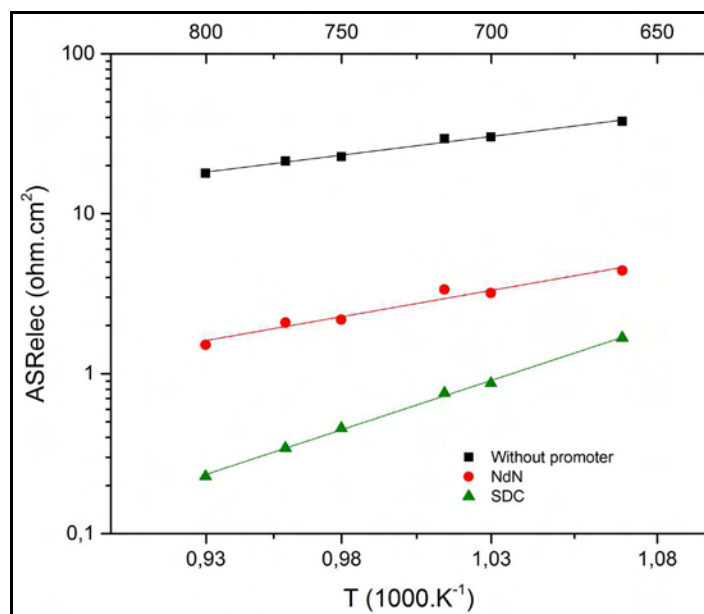

Figure 9. Evolution of the ASR_{elec} versus temperature of different promoters into a LSM backbone.
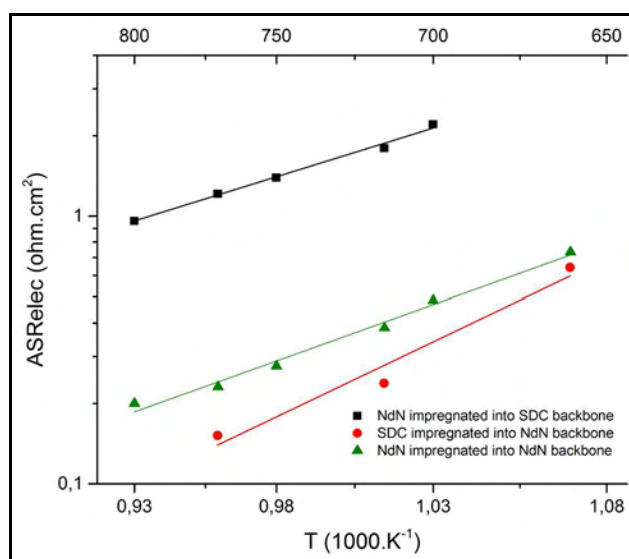
SDC Backbone

Figure 10. Comparison of the evolution of ASR_{elec} versus temperature for impregnated NdN and SDC backbones.

A SDC backbone has been infiltrated with an NdN promoter and the ASR_{elec} measured has been compared in figure 10 with its opposite configuration (SDC into NdN) and with NdN into NdN (influence of backbone). The ASR_{elec} of NdN impregnated into SDC at 700°C is 2.21 $\Omega.cm^2$, whereas the values for the NdN backbones are lower than ASR_{elec}=0.4 $\Omega.cm^2$ at the same temperature. It can be clearly deduced that the MIEC NdN backbone seems more efficient than the pure ionic SDC one, the values of the ASR_{elec} of SDC backbone-sample being much higher than the others. The additional electronic conductivity of MIEC backbones facilitates the electrochemical processes relative to oxygen dissociation and ion conduction.

Application to Single SOFC

NdN backbones have been screen-printed onto commercial SOFC half-cell (YSZ-NiO/YSZ, 60x60 mm²) (see figure 11). For convenient reasons in order to avoid any contamination of the hydrogen electrode layer with the promoter solution, the painting method has been used to infiltrate a SDC promoter inside the air electrode backbone.

Figure 11. SOFC cell (60 x 60 mm²) with SDC-infiltrated NdN backbone electrode.
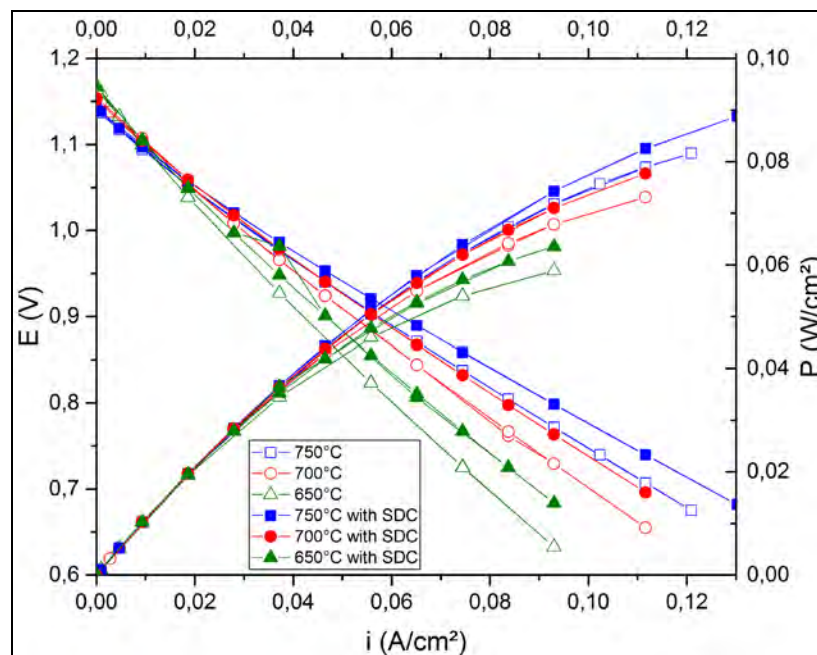

Figure 12. Electrochemical measurements performed on complete cells with and without infiltrated electrodes.

Figure 12 represents the I-V and I-P characteristics of the SOFC cells at different operation temperatures, one sample with non-infiltrated NdN air electrode (empty

symbols), and the other one with a SDC-impregnated NdN backbone (full symbols). Whatever the temperature, the ASR_{pol} deduced from impedance spectra of the impregnated sample is lower than in the case of the non-impregnated cell, corresponding to an improvement of the power density of 6 % at 700°C (P=78mW/cm² and P=73mW/cm², respectively), even higher (8%) at 750°C (P=89mW/cm² and P=82mW/cm², respectively). These results obtained on non-optimized samples could be significantly improved by the impregnation of PrN instead of SDC and the use of the vacuum-assisted infiltration process.

Conclusion

Nano-structured cathodes have been fabricated by promoter impregnation process into specific porous backbones: LSM as pure electronic conductor, SDC as pure ionic conductor and NdN as mixed ionic and electronic conductor. Several promoter compositions have been studied to evaluate the influence of the infiltrated material. The comparison between a simple painting method and the complete vacuum-assisted impregnation indicated that the vacuum helps the insertion of the promoter inside the porous backbone. The PrN promoter impregnated into an NdN backbone sample presented the lowest ASR_{elec} at 700°C (ASR_{elec}=0.26 $\Omega.cm^2$). Among three specific backbones studied, the lowest ASR_{elec} were measured on the infiltrated mixed ionic and electronic conductor NdN. Finally, complete single SOFC with and without infiltrated air electrodes have been manufactured and the infiltration clearly improved the efficiency of the cell, more than 6% in the temperature range 650-750°C without optimization.

References

1. S.P. Jiang, Int. *J. Hydrogen Energy*, **37**, 449 (2012).
2. R.P. Dowd Jr., S. Lee, Y. Fan, and K. Gerdes, *Int. J. Hydrogen Energy*, **41**, 14971 (2016).
3. S.P. Jiang, *Mater. Sci. Eng. A-Struct. Mater. Prop. Microstruct. Process*, **418**, 199 (2006).
4. R.J. Gorte and J.M. Vohs, J. Catal., **216**, 477 (2003).
5. Y. Chen, J. Bunch, C. Jin, C. Yanga and F. Chen, *J. Power Sources*, **204**, 40 (2012).
6. S. Ovtar, M. Chen, A.J. Samson and R. Kiebach, *Solid State Ionics*, **304**, 51 (2017).
7. X. Chen, Z. Tao, G. Hou, N. Xu and Q. Zhang, *Electr. Acta*, **165**, 142 (2015).
8. C. Lalanne, *PhD, University of Bordeaux* (2005).
9. X. Xu, C. Cao, C. Xia, and D. Peng, *Ceram. Int.*, **35**, 2213 (2009).
10. X. Xu, C. Xia, G. Xiao and D. Peng, *Solid State Ionics*, **176**, 1513 (2009).
11. F. Mauvy, C. Lalanne, J.-M. Bassat, J.-C. Grenier, H. Zhao, P. Dordor and P. Stevens, *J. Eur. Ceram. Soc.*, **25**(12), 2669 (2005).
12. C. Lalanne, G. Prosperi, J.-M. Bassat, F. Mauvy, S. Fourcade, P. Stevens, M. Zahid, S. Diethelm, J. Van Herle and J.-C. Grenier, *J. Power Sources*, **185**(2), 1218 (2008).
13. J.S.A. Carneiro, R.A. Brocca, M.L.R.S. Lucena and E. Nikolla, *App. Cat. B: Env.*, **200**, 106 (2017).

14. C. Nicollet, A. Flura, V. Vibhu, A. Rougier, J.-M. Bassat and J.-C. Grenier, *J. Power Sources*, **294**, 473 (2015).
15. X. Zhang, H. Zhang and X. Liu, *J. Power Sources*, **269**, 412 (2014).
16. D. Mesguich, J.-M. Bassat, C. Aymonier, A. Brüll, L. Dessemond and E. Djurado, *Electrochem. Acta*, **87**, 330 (2013).
17. C. Ferchaud, J.-C. Grenier, Y. Zhang-Steenwinkel, M.M.A. van Tuel, F.P.F. van Berkel and J.-M. Bassat, *J. Power Sources*, **196**, 1872 (2011).
18. D.J. Buttrey, P. Ganguly, J.M. Honig, C.N.R. Rao, R.R. Schartman and G.N. Subanna, *J. Solid State Chem.*, **74**, 233 (1988).
19. X. Lou, S. Wang, Z. Liu, L. Yang and M. Liu, *Solid State Ionics*, **180**(23–25), 1285 (2009).
20. F.S. Baumann, J. Maier and J. Fleig, *Solid State Ionics*, **179**(21–26), 1198 (2008).
21. S. Yin,M. Li, Y. Zeng, C. Li, X. Chen and Z. Ye, *J. Rare Earths*, **32**, 767 (2014).
22. K. Chen, Z. Lü, X. Chen, N. Ai, X. Huang, X. Du and W. Su, *J. Power Sources*, **172**(2), 742 (2007).
23. R. Tian, J. Fan, Y. Liu and C. Xia, *J. Power Sources*, **185**(2), 1247 (2008).
24. F. Bidrawn, G. Kim, N. Aramrueang, J.M. Vohs and R.J. Gorte, *J. Power Sources*, **195**(3), 720 (2010).
25. B. Huang, X.-J. Zhu, Y. Lv and H. Liu, *J. Power Sources*, **209**, 209 (2012).
26. B. Hee Kim, Q. Xu, B.K. Ahn, W.J. Kang and D.P. Huang, *Ceram. Int.*, **35**, 1335 (2009).